Title

cotH Genes Are Necessary for Normal Spore Formation and Virulence in Mucor lusitanicus

Journal

mBio, 14(1)

ISSN

2161-2129

Authors

Szebenyi, Csilla
Gu, Yiyou
Gebremariam, Teclegiorgis
et al.

Publication Date

2023-02-28

DOI

10.1128/mbio.03386-22

Peer reviewed

AMERICAN SOCIETY FOR MICROBIOLOGY | mBio®

RESEARCH ARTICLE

cotH Genes Are Necessary for Normal Spore Formation and Virulence in *Mucor lusitanicus*

Csilla Szebenyi,[a,b] Yiyou Gu,[c] Teclegiorgis Gebremariam,[c] Sándor Kocsubé,[a,b] Sándor Kiss-Vetráb,[a,b] Olivér Jáger,[a,b] Roland Patai,[d] Krisztina Spisák,[d,e] Rita Sinka,[f] Ulrike Binder,[g] Mónika Homa,[a,b] Csaba Vágvölgyi,[a,b] Ashraf S. Ibrahim,[c,h] Gábor Nagy,[a,b] Tamás Papp[a,b]

[a]Department of Microbiology, University of Szeged, Szeged, Hungary
[b]ELKH-SZTE Fungal Pathomechanisms Research Group, Faculty of Science and Informatics, University of Szeged, Szeged, Hungary
[c]Division of Infectious Diseases, The Lundquist Institute for Biomedical Innovation at Harbor-University of California Los Angeles (UCLA) Medical Center, Torrance, California, USA
[d]Institute of Biophysics, Biological Research Centre, Szeged, Hungary
[e]Doctoral School of Theoretical Medicine, University of Szeged, Szeged, Hungary
[f]Department of Genetics, University of Szeged, Szeged, Hungary
[g]Institute of Hygiene and Medical Microbiology, Medical University of Innsbruck, Innsbruck, Austria
[h]David Geffen School of Medicine at UCLA, Los Angeles, California, USA

Gábor Nagy and Tamás Papp contributed equally to this work.

ABSTRACT Mucormycosis is an invasive fungal infection caused by certain members of the fungal order of Mucorales. The species most frequently identified as the etiological agents of mucormycosis belong to the genera *Rhizopus*, *Lichtheimia*, and *Mucor*. The frequency of systemic mucormycosis has been increasing, mainly because of increasing numbers of susceptible patients. Furthermore, Mucorales display intrinsic resistance to the majority of routinely used antifungal agents (e.g., echinocandins and short-tailed azoles), which limits the number of possible therapeutic options. All the above-mentioned issues urge the improvement of molecular identification methods and the discovery of new antifungal targets and strategies. Spore coat proteins (CotH) constitute a kinase family present in many pathogenic bacteria and fungi and participate in the spore formation in these organisms. Moreover, some of them can act as virulence factors being receptors of the human GRP78 protein during *Rhizopus delemar*-induced mucormycosis. We identified 17 *cotH*-like genes in the *Mucor lusitanicus* genome database. Successful disruption of five *cotH* genes in *Mucor* was performed using the CRISPR-Cas9 system. The CotH3 and CotH4 proteins play a role in adaptation to different temperatures as well as in developing the cell wall structure. We also show CotH4 protein is involved in spore wall formation by affecting the total chitin content and, thus, the composition of the spore wall. The role of CotH3 and CotH4 proteins in virulence was confirmed in two invertebrate models and a diabetic ketoacidosis (DKA) mouse model.

IMPORTANCE Current treatment options for mucormycosis are inadequate, resulting in high mortality rates, especially among immunosuppressed patients. The development of novel therapies for mucormycosis has been hampered by lack of understanding of the pathogenetic mechanisms. The importance of the cell surface CotH proteins in the pathogenesis of *Rhizopus*-mediated mucormycosis has been recently described. However, the contribution of this family of proteins to the virulence of other mucoralean fungi and their functionality in vital processes remain undefined. Through the use of the CRISPR-Case9 gene disruption system, we demonstrate the importance of several of the CotH proteins to the virulence of *Mucor lusitanicus* by using three infection models. We also report on the importance of one of these

Editor Anuradha Chowdhary, Vallabhbhai Patel Chest Institute

Address correspondence to Tamás Papp, pappt@bio.u-szeged.hu, or Ashraf S. Ibrahim, ibrahim@lundquist.org.

The authors declare a conflict of interest. A.S.I. owns shares in Vitalex Biosciences, a start-up company that is developing immunotherapies and diagnostics for mucormycosis.

Received 8 December 2022
Accepted 14 December 2022
Published 10 January 2023

proteins, CotH4, to spore wall formation by affecting chitin content. Therefore, our studies extend the importance of CotH proteins to *Mucor* and identify the mechanism by which one of the CotH proteins contributes to the development of a normal fungal cell wall, thereby indicating that this family of proteins can be targeted for future development of novel therapeutic strategies of mucormycosis.

KEYWORDS mucormycosis, virulence factor, spore coat protein, CRISPR-Cas9, CotH, *Drosophila melanogaster*, *Galleria mellonella*, mice, *Mucor lusitanicus*, chitin, pathogenesis, virulence determinants

Mucormycosis is a life-threatening opportunistic fungal infection caused by several members of the order Mucorales (1). *Rhizopus*, *Lichtheimia*, and *Mucor* species have most often been isolated from such infections as the causative agents (2–6). These invasive infections, which can manifest as rhino-orbito-cerebral, pulmonary, gastrointestinal, cutaneous, or disseminated diseases, are known for their aggressive progression and high mortality rates (i.e., 30 to 90%, depending on the manifestation, the underlying condition of the patient, and the therapy) (5, 7, 8). They most frequently occur in patients with an immunocompromised status due to immunosuppression (i.e., primarily for solid organ or hematopoietic stem cell transplantation) or hematological malignancies. Uncontrolled diabetes (with or without ketoacidosis), elevated levels of free iron in the blood, and severe trauma can also be risk factors for mucormycosis (6, 7, 9, 10). The frequency of systemic mucormycosis has been increasing, mainly because of the increasing numbers of susceptible populations. Furthermore, Mucorales fungi display intrinsic resistance to the majority of routinely used antifungal agents (e.g., echinocandins and short-tailed azoles), which also limits the number of possible therapeutic options (4, 11). Recently, an increasing number of mucormycosis cases have been reported among COVID-19 patients treated with corticosteroids and with underlying diabetes (12–14).

Spore coat protein H (CotH) was first discovered in the endospore-forming bacterium *Bacillus subtilis* where it participates in the formation of the endospore coat (15). It proved to be an atypical protein kinase, which has an essential role in endospore formation by phosphorylating other structural proteins, such as CotB and CotG. Knockout of the encoding *cotH* gene had a pleiotropic effect on the structure of the outer spore coat, as well as the development of a germination-deficient phenotype (16–18).

CotH proteins not only occur in endospore-forming bacteria but also are present in many Mucoromycota species, such as *Mucor lusitanicus*, *Lichtheimia corymbifera*, *Cunninghamella bertholletiae*, *Rhizopus delemar*, *Saksanaea vasiformis*, *Syncephalastrum monosporum*, *Mortierella alpina*, and *Umbelopsis isabellina* (19, 20). In the mucormycosis-causing species *R. delemar* (synonym *R. oryzae*), several CotH proteins, including CotH1 (RO3G_05018 [EIE80313.1]), CotH2 (RO3G_08029 [EIE83324.1]), CotH3 (RO3G_11882 [EIE87171.1]), CotH4 (RO3G_09277 [EIE84567.1]), CotH5 (RO3G_01139 [EIE76435.1]), CotH6 (IGS-990-880_03186), CotH7 (IGS-990-880_09445), and CotH8 (IGS-990-880_11474), were previously identified (20, 21). Among them, CotH2 and CotH3 were found to mediate the interaction of the fungus with the glucose-regulated protein 78 (GRP78) expressed on the surface of endothelial cells (19), while CotH7 was found to mediate invasion of alveolar epithelial cells via interaction with integrin $\alpha 3\beta 1$ (22). This interaction proved to be crucial for the fungal invasion of the host. Specifically, the level of GRP78 molecules significantly increases in sinuses and lungs during diabetic ketoacidosis (DKA), causing vulnerability toward the fungal infection (23). Moreover, IgG antibodies produced against a peptide of *Rhizopus* CotH3 protein and conserved among CotH7 protein protected mice with DKA and neutropenia from mucormycosis (19). Thus, anti-CotH3 antibodies were proposed as promising candidates for immunotherapy of human mucormycosis (1). Finally, due to the universal presence of *cotH* genes in Mucorales and the lack of their presence in other pathogens, they proved to be appropriate biomarkers for diagnosis through a PCR-based assay allowing fungal DNA detection in human urine samples (24).

M. lusitanicus (formerly *Mucor circinelloides* f. *lusitanicus*) (25) is a frequently used model

TABLE 1 Genomic position and protein ID in JGI MycoCosm's database of the genes encoding the identified CotH-like proteins in *M. lusitanicus* and their names used in the study

Protein ID	Genomic location	Name in this study	Amino acid length (aa)	Signal sequence	GPI anchor predicted
1524506	scaffold_5:3666732–3669040	*cotH1*	555	+	−
1443041	scaffold_1:3072475–3074523	*cotH2*	621	+	+
109302	scaffold_3:4206378–4208599	*cotH3*	707	+	−
1501640	scaffold_4:354982–357045	*cotH4*	592	+	+
1507776	scaffold_4:2485275–2486992	*cotH5*	524	+	
1498659	scaffold_3:4206283–4208688	*cotH6*	569	+	−
1461483	scaffold_1:3050837–3053028	*cotH7*	594	+	−
1506605	scaffold_4:2063119–2065181	*cotH8*	589	+	−
1590338	scaffold_7:853960–855891	*cotH9*	595	+	−
1392021	scaffold_7:437729–439702	*cotH10*	570	+	+
1395371	scaffold_8:1812362–1814310	*cotH11*	596	+	−
1388805	scaffold_5:3661652–3663532	*cotH12*	607	+	+
1547701	scaffold_8:460886–463223	*cotH13*	590	+	−
1521260	scaffold_5:2598993–2601087	*cotH14*	581	+	−
1407491	scaffold_1:803076–804881	*cotH15*	581	+	−
1536541	scaffold_6:3298508–3300483	*cotH16*	524	+	−
1561577	scaffold_2:4842618–4846044	*cotH17*	590	+	−

organism for studying morphogenesis and pathogenesis of mucormycosis (26–31). In the genome of this fungus, we found 17 possible *cotH* genes, of which the function and role in the pathogenicity or other mechanisms are yet unknown. This high number of genes lets us consider the possibility that the CotH family may be a diverse group of proteins having a role in various biological processes. The present study aimed to investigate the function and possible role in pathogenicity of five *cotH* genes of *M. lusitanicus*.

RESULTS

***In silico* analysis of the CotH proteins.** In the *M. lusitanicus* genome database (DoE Joint Genome Institute; *M. lusitanicus* CBS277.49v3.0; [http://genome.jgi-psf.org/Mucci3/Mucci3.home.html]), 17 potential CotH-like protein-coding genes were found by a similarity search using the amino acid sequence of *R. delemar* 99–880 CotH1 (EIE80313.1), CotH2 (EIE83324.1), and CotH3 (EIE87171.1), which were named CotH1 to CotH17, respectively (Table 1). *In silico* analysis of the *M. lusitanicus* putative CotH proteins' amino acid sequences indicated that all of them carry the CotH kinase domain (Pfam ID PF08757), while there are 15 genes in the *Rhizopus delemar* genome that carry the CotH domain (Pfam ID PF08757) (15, 16). Furthermore, the *M. lusitanicus* CotH proteins are associated with the presence of a signal peptide, while only CotH2, CotH4, CotH10, and CotH12 contained sequences predicted to encode glycosylphosphatidylinositol (GPI)-anchored proteins. Analysis of the sequences suggests that CotH proteins can be predominantly extracellular in nature. Among the 17 putative proteins, only the amino acid sequences of CotH4, CotH5, and CotH13 carry the special (M/Q/A-E/M/A-QTNDGAY-I/K-D-T/Y/G-N/A/E-E/N/T-N) motif previously described in *R. delemar* CotH2 and CotH3 proteins as a ligand for the GRP78 receptor (Fig. 1) (18), thereby suggesting that these proteins might play a role in the virulence of *M. lusitanicus*.

All publicly available fungal genomic sequences were used for phylogenetic analysis of CotH proteins. The simplified view of the resulting tree is shown in Fig. 2, while the whole version can be found in Fig. S1 in the supplemental material. The collapse of the phylogenetic tree was based on the merging of clades of genes from predominantly closely related species. Interestingly, CotH proteins were found only in two phyla, Neocallimastigomycota and Mucoromycota, and within the latter, they were detected in two subphyla, Mucoromycotina and Mortierellomycotina. In the Mucoromycota linage, 12 well-supported clades with Mucorales CotH proteins occurred (Fig. 2). The remaining isolates, all of which were Neocallimastigomycetes, formed a distinct clade. Mortierellomycetes fungi are located in

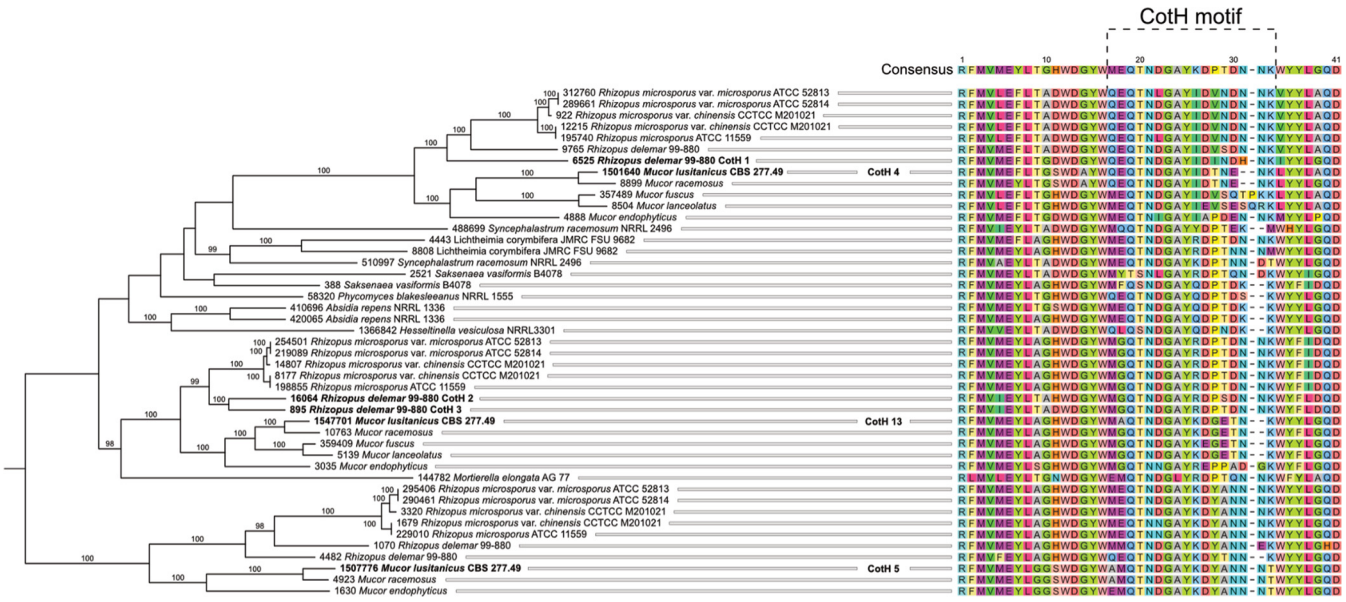

FIG 1 CotH motif-carrying proteins in Mucorales based on *in silico* analysis. The tree shows clade 1 of the full phylogeny based on the available fungal genomic sequences presented in Fig. S1.

a self-clade (clade 2), integrated between clade 1 and clade 3, formed by *Mucor* and *Rhizopus* isolates, respectively.

Mucor CotH4, CotH5, and CotH13, which carry the special amino acid sequence described as a ligand for the GRP78 receptor (18), were localized in the same clade (clade 1) together with the *Rhizopus* CotH2 and CotH3 proteins, which have been described previously for their essential role in virulence (Fig. 1) (18). Clade 1 also includes the *R. delemar* CotH7 (IGS-990-880_09445 [protein ID 9765]), which appears to be the major ligand mediating binding to integrin $\alpha 3 \beta 1$ of alveolar epithelial cells (22). Clade 3, clade 4, clade 5, clade 11, and clade 12 include both *Rhizopus* and *Mucor* CotH proteins, while some CotH proteins are segregated into clades formed exclusively by *Mucor* species (clade 7 and clade 8). Uniquely, in clade 1, some CotH homologues found in *M. lusitanicus* (i.e., CotH4, CotH5, and CotH13) are most closely related to the *R. delemar* and *P. blakesleeanus* orthologues than to their paralogs.

Transcription analysis of the *M. lusitanicus cotH* genes. Transcription of the 17 *cotH* genes was analyzed by real-time quantitative reverse transcription-PCR (qRT-PCR) on the second day of cultivation at 28°C (Fig. S2), where *cotH2* and *cotH4* showed the highest expression. Most *cotH* genes reached their maximum transcript abundance on the second day of cultivation at 28°C, the optimum temperature of the fungus. Interestingly, the transcription level of *cotH4* increased dramatically at higher glucose concentrations and in the presence of human serum (Fig. S2). Based on the qRT-PCR analysis, five genes (i.e., *cotH1* to *cotH5*) were selected for disruption and functional analysis.

Knockout of five *cotH* genes using the CRISPR-Cas9 system. Disruption of *cotH1*, *cotH2*, *cotH3*, *cotH4*, and *cotH5* was performed using a CRISPR-Cas9 system, and the resulting mutants were named MS12-Δ*cotH1*+*pyrG*, MS12-Δ*cotH2*+*pyrG*, MS12-Δ*cotH3*+*pyrG*, MS12-Δ*cotH4*+*pyrG*, and MS12-Δ*cotH5*+*pyrG*, respectively. For further analysis two independently derived mutants were selected. In each case, a template DNA containing the *pyrG* gene as a selection marker and two fragments homologous to the target site served as the deletion cassette. Transformation and genome editing frequencies are presented in Table S1A. In the experiments performed to disrupt the *cotH5* gene, transformed protoplasts died before the colony development or colonies could be maintained only temporarily, indicating that the disruption of this gene may be lethal for the fungus. It is also possible that the mutation causes a defect in protoplast regeneration; thus, transformants could not be recovered even though the mutant would be viable under normal growth conditions. Investigation of this possibility is hampered by the fact that currently only

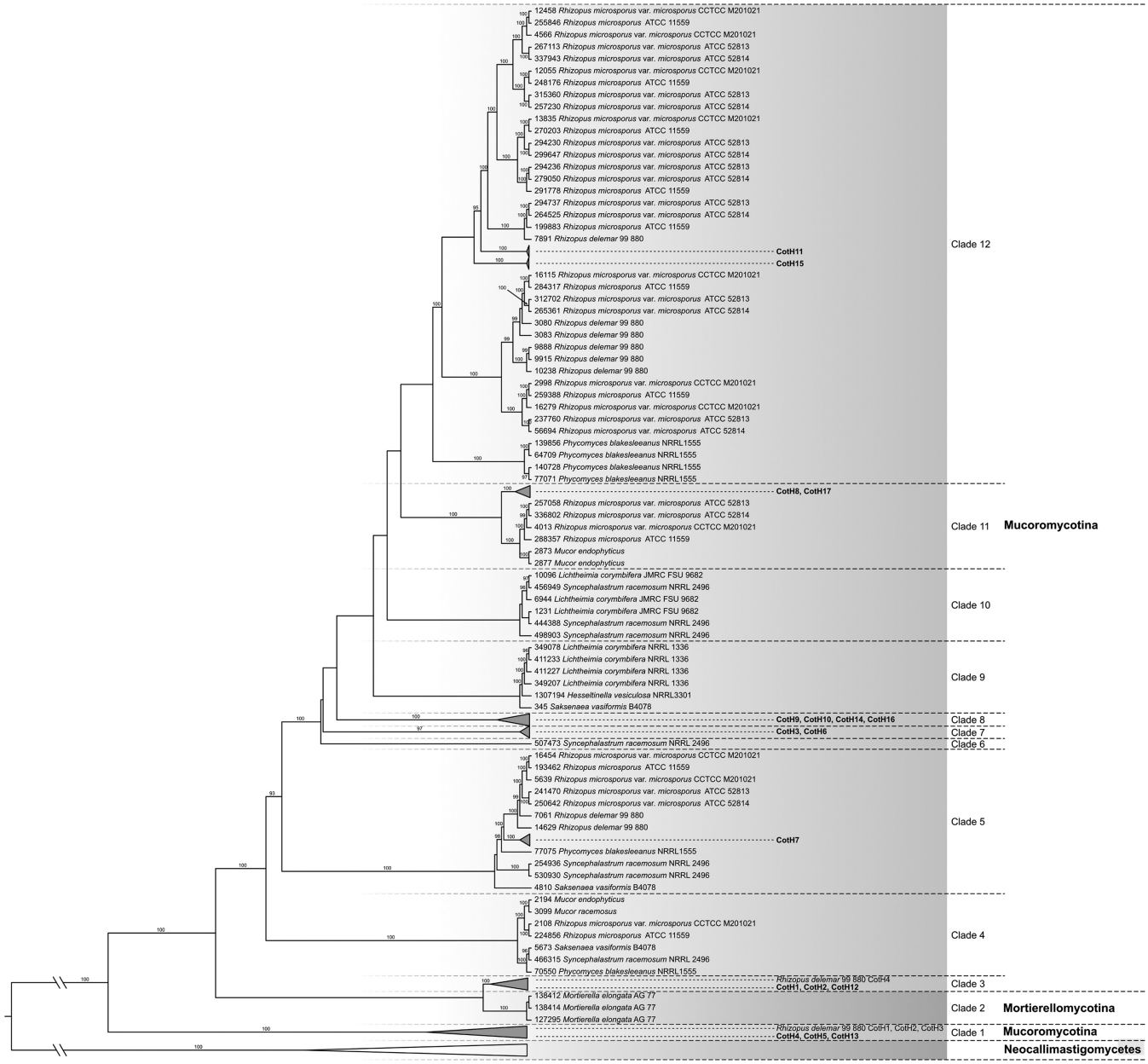

FIG 2 Collapsed version of the maximum likelihood tree showing phylogenetic relationships of *cotH* gene sequences. The simplified view of the maximum likelihood tree was based on the merging of clades of genes of predominantly closely related species. Only bootstrap values of >95% from maximum likelihood analyses are shown above the branches.

transformation of protoplasts of the fungus offers the possibility of producing stable genetic mutants of *M. lusitanicus*.

Characterization of the knockout mutants. (i) Growth ability of the mutants. The growth ability of the mutants was examined at 20, 28, and 35°C for 4 days. Growth analysis was performed with two independently derived mutants for each *cotH* knockout. No significant differences in the growth of MS12-Δ*cotH1*+*pyrG*, MS12-Δ*cotH2*+*pyrG*, and the control strain were observed at the optimum growth temperature of the fungus (28°C) (Fig. 3A). However, the colony diameter of MS12-Δ*cotH3*+*pyrG* significantly increased, while that of MS12-Δ*cotH4*+*pyrG* significantly decreased compared to the control strain at this temperature (Fig. 3A). Apart from the growth intensity of these two strains, the morphology of the mutants did not differ from that of the original strain. Cultivation at lower temperature did not affect the growth of the strains differently compared to the

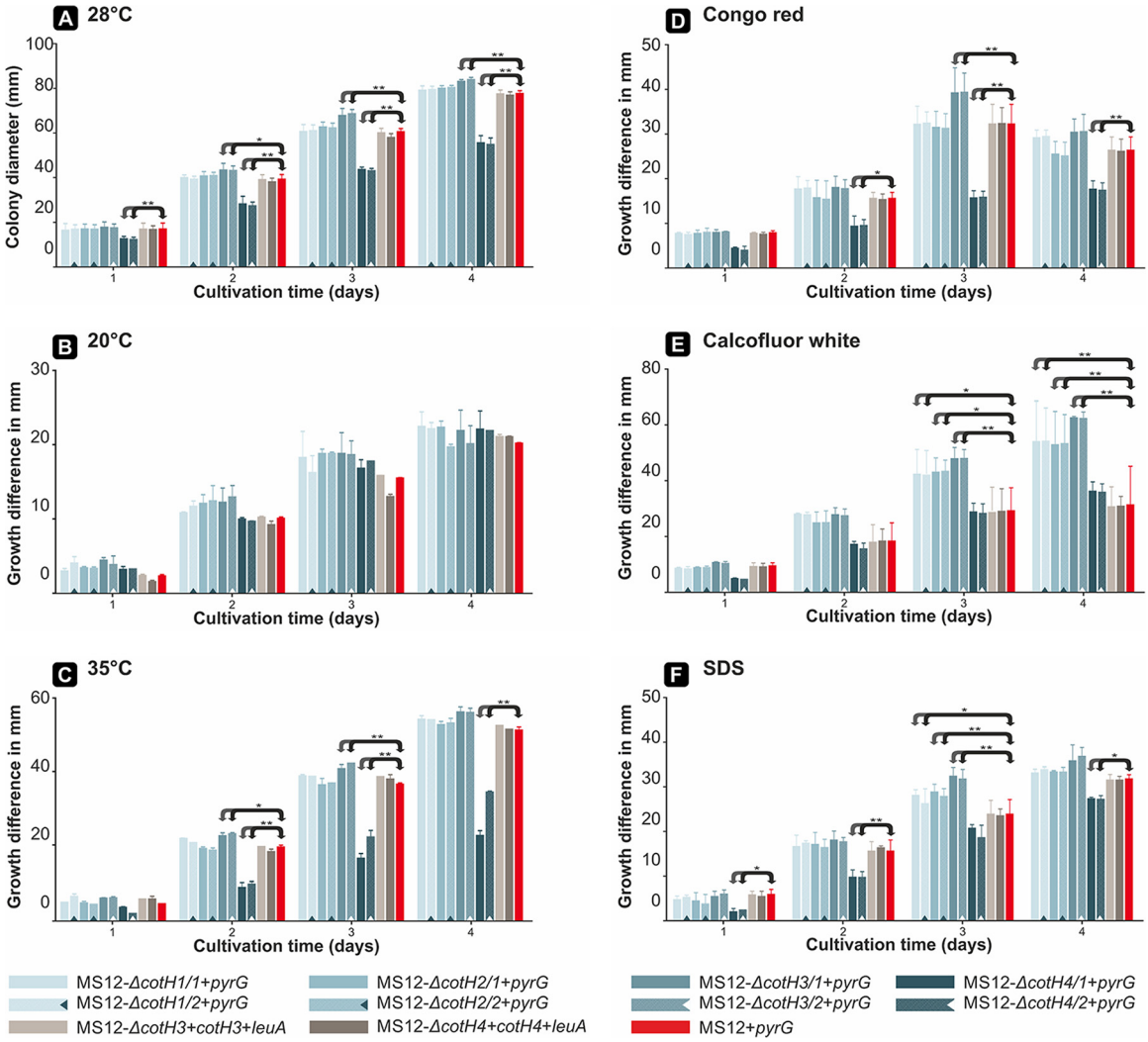

FIG 3 Growth of *cotH* mutants at different temperatures and effect of different stressors. (A) Colony diameter of the *cotH* mutant strains on leucine-supplemented minimal medium for 4 days at 28°C; (B) effect of the lower temperature on growth of *cotH* mutant strains on leucine-supplemented minimal medium for 4 days at 20°C; (C) effect of the higher temperature on growth of *cotH* mutant strains on leucine-supplemented minimal medium for 4 days at 35°C. The effects of the lower (B) and higher (C) temperatures on the growth of *cotH* mutant strains are represented by comparing the differences of the colony diameters measured after cultivation under the control conditions and those obtained in the cultivation under 20°C and 35°C. (D) Effect of Congo Red (CR) on the growth of *cotH* mutant strains; (E) effect of calcofluor white (CFW) cell wall stressor on the growth of *cotH* mutant strains; (F) effect of SDS membrane stressor on the growth of *cotH* mutant strains. The effects of the different stressors on the growth of the mutants are represented by comparing the differences of the colony diameters measured after cultivation under the control conditions and those obtained in the presence of the stressor. The values presented are from three independent cultivations (error bars indicate standard deviation). The strains were grown at 28°C in the dark for 4 days, and colony diameters were measured daily. The effects of the different temperatures (A to C) and stressors (D to F) were then plotted in millimeters, and significance was calculated based on the effect of the temperatures or stressors on MS12+*pyrG*. *P* values were calculated according to the two-sample paired *t* test statistical method. Values indicated by asterisks are significantly different from the value of the MS12+*pyrG* strain measured on the same day (*, $P \leq 0.05$; **, $P \leq 0.01$).

control (Fig. 3B). At 35°C, growth of the *cotH4* disruption mutant was significantly less affected by the increased temperature than those of the *cotH1*, *cotH2*, and *cotH3* mutants (Fig. 3C). Complementation of the *cotH3* or *cotH4* gene was achieved by an autosomally replicating plasmid construction, where the complementing gene construct was maintained extrachromosomally. After complementation of the *cotH3* and *cotH4* gene, the resulting MS12-Δ*cotH4*+*cotH4*+*leuA* strain showed the growth characteristics of the control (MS12+*pyrG*) (Fig. 3).

Cell wall stressors Congo Red (CR) and calcofluor white (CFW) had significant effects on the growth of all strains compared to cultivation on normal medium (Fig. 3). Difference of the colony diameter of each mutant from that of the control strain on normal, untreated

medium (Fig. 3A) (i.e., increased or decreased growth ability of the mutants) was taken into account during the evaluation. Using CR as a stressor, no difference in the growth intensity of the deletion mutants MS12-Δ*cotH1*+*pyrG* and MS12-Δ*cotH2*+*pyrG* was observed compared to MS12+*pyrG* (i.e., the control strain). MS12-Δ*cotH3*+*pyrG* displayed an increased sensitivity, while MS12-Δ*cotH4*+*pyrG* showed higher resistance to CR than the control strain (Fig. 3D). CFW exerted a significant effect on the growth of all *cotH* mutants. MS12-Δ*cotH1*+*pyrG*, MS12-Δ*cotH2*+*pyrG*, and MS12-Δ*cotH3*+*pyrG* was more sensitive, while MS12-Δ*cotH4*+*pyrG* was more resistant to CFW than MS12+*pyrG* (Fig. 3E). The MS12-Δ*cotH4*+*pyrG* proved to be more resistant to SDS than the control strain. The effect of SDS was observed from the third cultivation day in the case of MS12-Δ*cotH1*+*pyrG*, MS12-Δ*cotH2*+*pyrG*, and MS12-Δ*cotH3*+*pyrG* (Fig. 3F). For these strains, an increased sensitivity was observed. After complementation of the *cotH3* and *cotH4* gene, the resulting MS12-Δ*cotH3*+*cotH3*+*leuA* and MS12-Δ*cotH4*+*cotH4*+*leuA* strains showed the growth characteristics of the control (MS12+*pyrG*) (Fig. 3).

Under aerobic conditions, *M. lusitanicus* displays a hyphal growth, while it grows in a yeast-like form under anaerobiosis. This feature, named as morphological dimorphism is regarded as an important property of pathogenicity (27). Gene disruption did not affect the anaerobic growth of any of the mutants compared to the control strain, and yeast-like cells could be formed in the absence of the tested *cotH* genes. However, under microaerophilic conditions, MS12-Δ*cotH4*+*pyrG* produced more elongated hyphae than the control strain (Fig. S3).

(ii) Transmission electron microscopic analysis of the spores of the mutant strains. To determine the effect of the gene disruptions on the spore wall structure of *M. lusitanicus* spores of the mutants and the control strain (MS12+*pyrG*) were subjected to transmission electron microscopic (TEM) image analysis (Fig. 4). Spore wall of MS12-Δ*cotH4*+*pyrG* showed a characteristic phenotype as it was abnormally thickened (Fig. 4B and D and Data Set S1). After complementation of the *cotH4* gene disruption, the cell wall of MS12-Δ*cotH4*+*cotH4*+*leuA* spores was restored and the cell wall thickness of the complemented spores did not differ significantly from those of the control (MS12+*pyrG*) (Fig. S4).

(iii) Surface analysis of fungal spores with fluorescent dyes. By monitoring the spores stained with CWF, we found that the dye-emitted intensity of the spores of MS12-Δ*cotH4*+*pyrG* significantly increased compared to the control (Fig. S5) suggesting a chitin accumulation in the spore wall. At the same time, staining for mannosyl derivatives using concanavalin A-fluorescein isothiocyanate (ConA-FITC) did not reveal differences among the mutants and the control strain. Intensity of the *cotH4*-complemented (i.e., MS12-Δ*cotH4*+*cotH4*+*leuA*) spores did not differ significantly from those of the control (MS12+*pyrG*) (Fig. S5).

(iv) *In vitro* interaction with macrophages. To examine whether recognition and internalization of the fungal spores by macrophages were affected by the disruption of the *cotH* genes in *M. lusitanicus*, the phagocytosing capacity (Fig. S6) and the phagosome maturation of J774.2 cells exposed to the MS12+*pyrG* and the mutant strains were tested (Fig. S7). Subsequently, J774.2 cells were coincubated for 3 h with the labeled spores, and then the ratio of pHrodo Red$^+$ macrophages was examined by imaging flow cytometry (see Fig. S7A and B in the supplemental material). No significant differences were found between the mutant and the control strains in neither the phagocytic index values (Fig. S6C). Similarly, testing the survival of fungal spores cocultured for 3 h with murine J774.2 cells did not detect differences between the control and the mutant strains (Fig. S6D). Moreover, our results suggested that the viability of spores did not decrease in the presence of macrophages at all. Furthermore, acidification of phagosomes is not affected by the lack of the examined CotH proteins (Fig. S7B) and the absence of CotH proteins did not affect the survival of spores after *in vitro* interaction with macrophages.

(v) *In vivo* study of virulence of *cotH* mutant strains. To investigate the role of CotH proteins in pathogenicity of *M. lusitanicus*, *Drosophila melanogaster* and wax

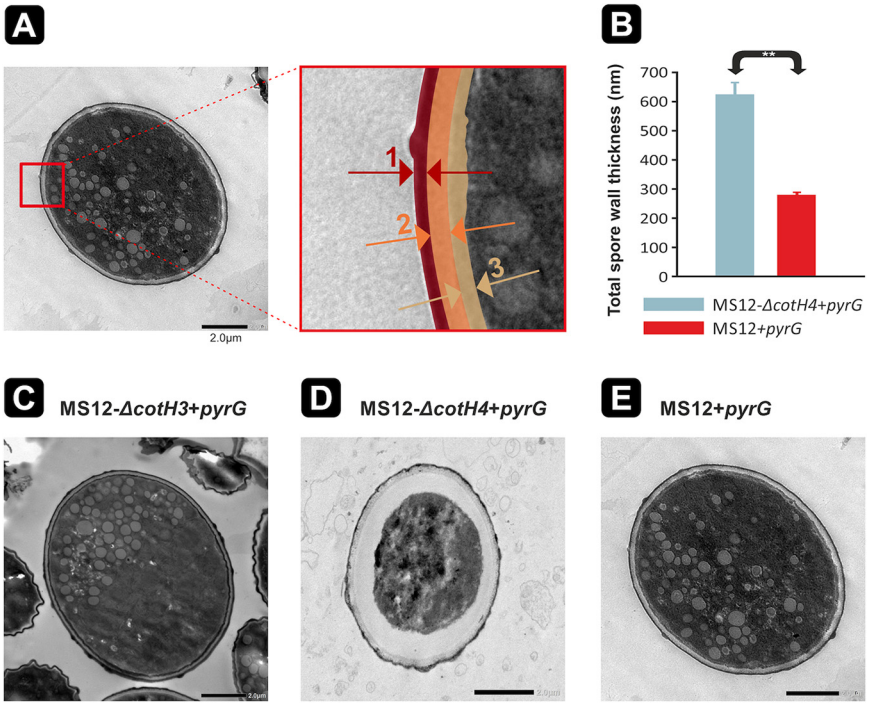

FIG 4 Cell wall changes of *cotH* mutants observed by TEM. (A) Schematic representation of the outer, inner, and middle layers of the cell wall of spores. TEM measurements represent the thickness of different cell wall layers, as shown in the right panel enlargement of the red box in the left panel of panel A: 1, outer spore wall layer; 2, middle spore wall layer; 3, inner spore wall layer. (B) Total spore wall thickness of layers 1 to 3 compared to the control strain. (C to E) Spores of the *cotH* mutants MS12-Δ*cotH3*+*pyrG* (C), MS12-Δ*cotH4*+*pyrG* (D), and MS12+*pyrG* (control) (E). Significance was calculated based on a two-sample *t* test (**, $P \leq 0.001$). Error bars indicate standard deviation. For each mutant, spore wall thickness was determined by measuring the thickness of five different spores at 10 different points on the spore wall. Scale bars, 2 μm.

moth larvae (*Galleria mellonella*) were used as nonvertebrate animal models in *in vivo* virulence studies.

In *D. melanogaster* (Fig. 5A), the pathogenicities of the control strain MS12+*pyrG* and the wild-type (WT) strain CBS277.49 did not differ significantly. However, lack of the *cotH3* and *cotH4* genes significantly decreased the virulence in the mutants compared to the controls. In case of the *Galleria* model Fig. 5B, disruption of the *cotH4* gene resulted in significantly decreased virulence of the mutant strain. In an intratracheally infected DKA mouse model, all the mice infected with the wild-type *M. lusitanicus* strain CBS277.4 died before the third day postinoculation (Fig. 5C). In this model, MS12-Δ*cotH3*+*pyrG* and MS12-Δ*cotH4*+*pyrG* showed significantly decreased virulence. After complementation of the *cotH3* and *cotH4* genes, the virulence of the resulting MS12-Δ*cotH3*+*cotH3*+*leuA* and MS12-Δ*cotH4*+*cotH4*+*leuA* strains showed the characteristics of the control (CBS277.49) (Fig. 5).

DISCUSSION

CotH protein-encoding genes are widely present in Mucorales fungi (19). Although present in other organisms, Mucorales *cotH* genes have divergent sequences from their orthologs in *Bacillus* species. However, the function of *cotH* genes has been verified in only a few of them (e.g., *B. subtilis*, *Bacillus cereus* and *R. delemar*) (15, 16, 19, 32). For instance, the *Rhizopus* CotH3 carries the amino acid sequence MGQTNDGAYRDPTDNN, which is assumed to be a key factor in the specific interaction between the fungal cells and the host's endothelial cells via the GRP78 molecule (19). This interaction was shown to be critical in enhancing *R. delemar* virulence through promotion of hematogenous dissemination (18). Equally important, the ability of *R. delemar* spores to invade

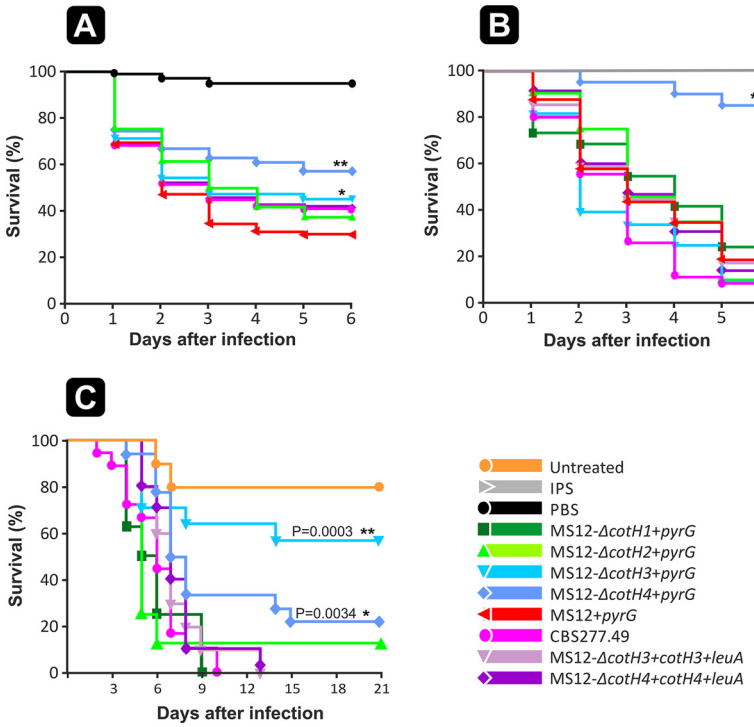

FIG 5 Virulence studies with *cotH* mutants. (A) Survival of *Drosophila melanogaster* ($n = 60$) infected with the *cotH* mutants and the control *M. lusitanicus* MS12+*pyrG* and CBS277.49 strains. Survival curves followed by asterisks were significantly different from the control strain (MS12+*pyrG*) according to the Mantel-Cox log rank test (*, $P \leq 0.05$; **, $P \leq 0.001$). The results from 3 independent experiments are summarized. (B) Survival of *Galleria mellonella* ($n = 20$) infected with the *cotH* mutants and the control *M. lusitanicus* MS12+*pyrG* and CBS277.49 strains. Survival curves followed by asterisks were significantly different from the control strain according to the Mantel-Cox log rank test (**, $P \leq 0.001$). The results from 3 independent experiments are summarized. (C) Virulence of *cotH* mutants in a DKA mouse model following intratracheal infection. DKA male ICR (CD-1) outbred mice (≥20 g) (Envigo) ($n = 8$) were infected intratracheally with 2.5×10^6 fresh spores (1×10^8 spores/mL) in 25 μL PBS. The results summarize the results of 2 independent experiments. Survival curves followed by asterisks were significantly different from the control strain according to the Mantel-Cox log rank test (*, $P \leq 0.05$; **, $P \leq 0.01$).

and damage nasal epithelial cells was directly proportional to the expression of GRP78 on nasal epithelial cells triggered by host conditions mimicking hyperglycemia and ketoacidosis, thus explaining the increased susceptibility of diabetics in ketoacidosis to the rhino-orbito-cerebral form of mucormycosis (ROCM) (22). Concordant with these findings, is the increased number of mucormycosis cases (mainly ROCM) detected among COVID-19 patients treated with corticosteroids and with underlining diabetes (i.e., COVID-19-associated mucormycosis [CAM]) (33). Interestingly, significantly higher serum GRP78 levels in COVID-19 patients have been reported and could explain the increased incidents of CAM through CotH/GRP78-mediated invasion of host tissues (34). Thus, some members of the CotH protein family serving as ligands for GRP78 receptors may be considered potential therapeutic targets (1).

In a previous study, several different *cotH* transcripts were reported to be expressed in *M. lusitanicus* using the domain profile PF08757 (34). Moreover, it was also noted that the number of *cotH* transcripts was 2 times higher in the transcriptome of *Mucor* strains considered to be pathogenic than in *Mucor* strains used in cheese production (35). This study used the so-called "CotH motif" described previously for *Rhizopus* (35) to report on the presence of three CotH proteins in *M. lusitanicus*. In our study, we found 17 genes in *M. lusitanicus* that contain the PF08757 domain, of which three genes (i.e., *cotH4*, *cotH5*, and *cotH13*) harbor the CotH motif. In the phylogeny of the *cotH* genes, *M. lusitanicus cotH4*, *cotH5*, and *cotH13* localized in the same clade (clade 1) together with the *R. delemar cotH2* and *cotH3* genes. Only the genes positioned in clade 1

of this phylogeny contained the CotH motif, suggesting that these genes may have a role in the CotH-GRP78 interaction.

Expression of the *M. lusitanicus* CotH3 protein proved to be essential for the virulence in the DKA mouse model. However, the encoding gene localizes to clade 7 along with the genes for other CotH proteins and does not carry the CotH motif predicted to interact with GRP78. This result suggests that host targets other than GRP78 are involved in mucormycosis pathogenesis due to *M. lusitanicus*. Indeed, integrin $\alpha 3\beta 1$ has been reported to be the target for *R. delemar* CotH7, which results in activation of the epidermal growth factor receptor (22, 36).

Phylogenetic analysis indicated that CotH proteins show a strong dominance in the Mucoromycotina fungi within the fungal kingdom. Clade 4, clade 5, clade 11, and clade 12 include both *Rhizopus* and *Mucor cotH* genes, while some *cotH* genes are segregated into clades formed exclusively by *Mucor* species (clade 7 and clade 8), suggesting various gene duplication events within the Mucoromycota clade. Distribution of the genes in the phylogeny also suggests that several duplication events may occur in the zygomycete ancestor before the divergence of species. The presence of this large number of genes and their phylogenetic analysis led us to consider the possibility that the CotH family is a diverse group of proteins, which may be involved in many biological processes and not exclusively in the virulence.

Since orthologs of CotH proteins are mostly considered spore surface or spore envelope structural elements (35), the spore wall composition of the fungus and its mutants generated in this study was monitored. TEM images revealed the separation of the spore wall and the cell membrane of the *cotH4* disruption mutant. Analysis using fluorescent dyes specifically binding to the cell wall components (37, 38) indicated a chitin accumulation between the two structures. Changes in the cell wall composition can alter the susceptibility to cell wall stressors, such as CFW and CR (37), and may influence the fungal virulence (39). Indeed, disruption of the *cotH4* gene decreased the sensitivity to CR and caused resistance to other stressors (i.e., CFW and SDS) at the same time, MS12-Δ*cotH3*+*pyrG* displayed an increased sensitivity to CR. The ability of pathogenic fungi to respond to stress is crucial in adapting to the host environment (40). Our results suggest that the proteins encoded by the *cotH3* and *cotH4* genes are involved in the determination of the spore wall composition and structure.

Chemical components, such as the surface molecules, and physical properties, such as the size and shape, of the fungal propagules greatly influence pathogen recognition and further removal of the fungus by the immune cells (41). Changes in the spore wall of the *cotH4* disruption mutant, as well as the absence of the CotH proteins, did not affect their recognition by the macrophages; also, no significant difference was found in the number of fungal cells phagocytosed by a macrophage. The ability of the spores to germinate and penetrate the cells determines the further outcome of the infection (41). It was previously described that *Mucor* spores within the phagosome are exposed to a cytotoxic environment, which includes acidification, nutrient starvation, oxidation, and the presence of antimicrobial proteins (41). We examined whether the acidification of phagosomes could be affected by the CotH proteins. In our experiments, macrophages were equally capable of killing the spores of the *cotH* knockout mutants, so neither the recognition nor the killing mechanism was impaired or altered. Despite the involvement of CotH proteins in cell wall remodeling and/or integrity, there is no indication that CotH1 to -4 proteins would be involved in phagosome maturation blockade in *Mucor*, as suggested by a previous study (41). It should be noted, however, that of the 17 CotH proteins encoded in the *Mucor* genome, two other proteins (i.e., ID 76509 [CotH8] and ID 166651 [CotH17]) are suggested to play a role in macrophage interactions (41).

Although the information on the role of genes or proteins involved in infection can be obtained through *in vitro* experiments, the function of systemic infection can only be elucidated in an *in vivo* model (42). Disruption of both the *cotH3* and the *cotH4* genes caused reduced virulence in the *Drosophila* infection model, while the disruption of *cotH1* and *cotH2* genes did not affect the virulence of the fungus. The *Drosophila* pattern

recognition receptors after the recognition of conserved microbial patterns can activate a cellular and humoral response that is specific to a particular microorganism (43). The wax moth, *G. mellonella*, is also a widely used nonvertebrate model organism to examine the pathogenicity of different filamentous fungi such as Mucorales species (26, 31, 44). *In vivo* viability studies in *G. mellonella* also confirmed the role of the CotH4 protein in virulence. The pathological alterations that resemble human mucormycosis are limited if we would like to use *Drosophila* or *Galleria*, but each of these is an appropriate model for testing larger numbers of mutants (42). Furthermore, there one limitation on the use of invertebrate hosts is whether the results obtained in these models can be adapted to mammals and the human body because of fundamental differences, such as the lack of an adaptive immune system and specific organs (42).

Inhalation of Mucorales spores is the most common route of infection. Thus, intratracheal instillation or intranasal inhalation is the most widely used models to mimic pulmonary infection. Disseminated mucormycosis can also be induced by intravenous inoculation of the fungus, usually into the tail vein and mimicking direct inoculation into the blood as the infection occurs in severe trauma (45). Therefore, the role of *cotH* genes in *R. delemar* was investigated using a DKA mouse model, in which pulmonary mucormycosis was induced by intratracheal instillation of fungal spores (19). This model is preferably used to investigate the pathomechanism of mucormycosis, as the most common underlying condition of this fungal disease is diabetic ketoacidosis in addition to immunodeficiency (3, 30, 38). For *M. lusitanicus*, an intratracheal mouse infection model had not been previously used, so the infectivity of the wild type (WT) (CBS277.4) in mice was first established (31). Viability studies in DKA mice demonstrated that deletion of either the CotH3 or CotH4 gene attenuates the pathogenicity of *M. lusitanicus*. Importantly, the *cotH3* mutant did not show reduced virulence in a *Galleria mellonella* model but did in a DKA mouse model with elevated GRP78 receptor expression, although the protein does not carry the characteristic motif determined earlier for *R. delemar*. The data suggest that *cotH* mutants exhibit altered cell wall composition or organization, with the *cotH4* mutant showing a significant loss of cell wall integrity and cell wall chitin composition. Host recognition of the fungal cell wall often determines the outcome in the host and plays an important role in the pathomechanism of the infection. Based on these findings, it seems conceivable that in *M. lusitanicus*, CotH3 and CotH4 proteins mediate the process of fungal infection in a cell-wall-dependent manner.

Spore size dimorphism is linked to virulence of *M. lusitanicus* species (24). However, considering that the mutant lacking the CotH3 protein showed reduced virulence in the pathogenicity studies, but no change in spore size, it can be assumed that spore size is not the only determining factor of virulence. Interestingly, interaction with the GRP78 receptor is unlikely in case of this mutant, as the CotH3 protein does not carry the CotH motif. Alternatively, other motifs that are yet to be identified bind to GRP78. Due to its sequence similarity to the *Rhizopus* CotH3 and the presence of the CotH motif, CotH4 could be a potential ligand for the GRP78 receptor, which requires further investigation. Given that CotH proteins are involved not only in pathogenicity but also in spore structure, it is important to consider the role of CotH protein family members not only as virulence factors but also in spore formation and other physiological roles.

MATERIALS AND METHODS

Strains, media, and growth conditions. Strain MS12 of *Mucor lusitanicus* (formerly known as *Mucor circinelloides* f. *lusitanicus*), which is auxotrophic to leucine and uracil (*leuA*$^-$ and *pyrG*$^-$) and was derived from strain CBS277.49 by chemical mutagenesis (46), was used in the transformation experiments. As the lack of a functional *pyrG* gene slightly affects the growth and virulence of *M. lusitanicus* (47), the strain MS12+*pyrG*, was used as a control during the characterization of mutants. In this strain, uracil auxotrophy was complemented by expressing the *pyrG* gene (47). In certain experiments, CBS277.49 was also involved as a control. Growth analysis was performed with two independently derived mutants for each of the *cotH* mutations.

For quantitative PCR (qPCR) experiments, human serum was isolated from venous blood of the same donors taken into serum separation blood collection tubes (BD Vacutainer, Becton Dickinson, Franklin Lakes, NJ, USA). Then, coagulation tubes were centrifuged at 300 × *g* for 15 min at room temperature

and the serum was collected and added at 10%, and then cultivation was performed for 2 days at 28°C in liquid minimal medium.

For nucleic acid extractions, spores were plated onto yeast nitrogen base (YNB) solid minimal medium consisting of 10 g/L glucose, 0.5 g/L yeast nitrogen base without amino acids (BD Difco, Becton, Dickinson, Franklin Lakes, NJ, USA), 1.5 g/L $(NH_4)_2SO_4$, 1.5 g/L sodium glutamate, and 20 g/L agar, supplemented with leucine and/or uracil (0.5 mg/mL) if required, and incubated at 28°C for 4 days. To test the mitotic stability of the transformants, malt extract agar (MEA) (10 g/L glucose, 5 g/L yeast extract, 10 g/L malt extract, and 20 g/L agar) was used as a complete, nonselective medium. To examine the effect of the temperature on the growth, 10^4 spores were plated on solid YNB and incubated at 20, 28, and 35°C. Anaerobic growth was performed in a BBL GasPak anaerobic system (Becton, Dickinson) with Anaerocult A (Merck, Darmstadt, Germany) at 28°C. Microaerophile growth was performed in a BBL GasPak anaerobic system (Becton, Dickinson) with Anaerocult C (Merck, Darmstadt, Germany) at 28°C, where 10^4 spores were plated on solid YNB and incubated at 28°C for 2 days. Fungi grown on YNB under anaerobiosis were sampled on the second day of culture, and the morphology of the fungal cells was examined by light microscopy. To determine the effect of membrane and cell wall stressors, 10^4 spores were point inoculated at the center of YNB with or without the stressors, which were SDS (4 mg/mL), Congo red (CR) (2 mg/mL), and calcofluor white (CFW) (0.1 mg/mL). For growth tests, plates were incubated at 28°C for 4 days in the dark, and colony diameter was measured daily. In each case, the difference between the colony diameters of the mutant strains and that of the control was determined under the control conditions (i.e., when the strains were grown at 28°C on YNB) and in the presence of the stressor. The effect of the different temperatures and stressors on the growth of the mutants was represented by comparing the differences in the colony diameters measured after cultivation under the control conditions and those obtained in the cultivation under stressors. The effect of the different temperatures was then plotted in millimeters, and significance was calculated based on the cultivation under different temperatures on MS12+*pyrG*.

Sequence and phylogenetic analysis of CotH proteins. Motifs, domains, and main features of the CotH proteins were predicted using the tools available at the Expasy Bioinformatics Resource Portal (http://www.expasy.ch), such as Compute pI/M_w, MyHits, PROSITE, and ProtScale (48). For the phylogenetic analysis, a blastp search was conducted on the JGI MycoCosm portal (https://mycocosm.jgi.doe.gov/mycocosm/home) (49) with 17 sequences of *Mucor lusitanicus* CBS277.49 containing the CotH domain. All retrieved sequences were scanned for CotH domains with InterProScan 5.48–83.0 (50) based on the Pfam database (51). Only those sequences were retained that contained CotH domains solely. Filtered sequences were clustered by using MMseq2 v.bbd564172bd55d9e6acd1170e59790c37157a21b (52) with default settings. Multiple-sequence alignment was conducted using MAFFT v.7.453 (53) with the E-INS-i iterative refinement method, including sequences from all clusters that contained the CotH domain based on the clustering results. Phylogenetic reconstruction was carried out by using IQ-TREE v.1.6.12 (54) with the LG4M+R7 model determined by the inbuilt ModelFinder tool (55). Statistical support of the best tree was calculated with ultrafast bootstrap approximation (56) in 5,000 replicates.

General molecular techniques. Genomic DNA and total RNA were isolated using the ZR Fungal/Bacterial DNA MiniPrep (Zymo Research, Irvine, CA, USA) and the Direct-zol RNA MiniPrep (Zymo Research, Irvine, CA, USA) kits, respectively, according to the instructions of the manufacturer. To amplify genes or gene fragments from genomic DNA, Phusion high-fidelity DNA polymerase (Thermo Fisher Scientific, Waltham, MA, USA) was used according to the manufacturer's recommendations. PCR products were isolated and concentrated using the Zymoclean large-fragment DNS recovery kit (Zymo Research, Irvine, CA, USA) and DNA Clean & Concentrator-5 (Zymo Research, Irvine, CA, USA). Restriction digestions and ligations were carried out according to the commonly used methods (57). To clone the PCR fragments, the pJET1.2/blunt vector (CloneJET PCR cloning kit; Thermo Fisher Scientific, Waltham, MA, USA) was used according to the manufacturer's instructions. Plasmid purification was carried out using the GeneJET plasmid miniprep kit (Thermo Fisher Scientific, Waltham, MA, USA) according to the manufacturer's recommendations. Sequencing of the cloned fragments was commercially performed by LGC Genomics (Berlin, Germany). The sequences obtained were aligned by using the BioEdit 7.2 sequence editor program (58) and analyzed using the Basic Local Alignment Search Tool (BLAST) at the site of the National Center for Biotechnology Information (NCBI) (https://blast.ncbi.nlm.nih.gov/Blast.cgi). Oligonucleotide sequences were designed based on the sequence data available in the *M. lusitanicus* CBS277.49 v.3.0 genome database (DoE Joint Genome Institute [http://genome.jgi-psf.org/Mucci2/Mucci3.home.html]) (59). Primers used in the study are listed in Table S1B in the supplemental material.

qRT-PCR analysis. Reverse transcription was carried out with the Maxima H minus first-strand cDNA synthesis kit (Thermo Fisher, Waltham, MA, USA) using random hexamer and oligo$(dT)_{18}$ primers according to the manufacturer's recommendations. qRT-PCR experiments were performed in a CFX96 real-time PCR detection system (Bio-Rad) using the Maxima SYBR green qPCR master mix (Thermo Fisher Scientific, Waltham, MA, USA), and the primers are presented in Table S1B. Relative quantification of copy number and gene expression was performed by the threshold cycle ($2^{-\Delta\Delta CT}$) method using the *M. lusitanicus* actin gene (CBS277.49 v.2.0 genome database, scaffold_07:2052804–2054242) as a reference (60). Amplification conditions involved 95°C for 3 min followed by 40 cycles at 95°C for 15 s, 60°C for 30 s, and 72°C for 30 s. Melting curve analysis was performed at 65 to 95°C with a 0.5°C increment. All experiments were performed in biological and technical triplicates.

Knockout of the *cotH* genes using the CRISPR-Cas9 method. Knockout mutants were constructed by partially exchanging the coding regions of the *cotH* genes to a functional *pyrG* gene (CBS277.49. v2.0 genome database ID Mucci1.e_gw1.3.865.1), which complements the uracil auxotrophy of the applied strain. This gene replacement was carried out by homology-driven repair (HDR) following a CRISPR-Cas9

strategy described previously (29, 61). Protospacer sequences designed to target the DNA cleavage in the *cotH1*, *cotH2*, *cotH3*, *cotH4*, and *cotH5* genes are presented in Table S2A. Using these sequences, Alt-R CRISPR RNA (crRNA) and Alt-R CRISPR-Cas9 transactivating crRNA (tracrRNA) molecules were designed and purchased from Integrated DNA Technologies (IDT, Coralville, IA, USA). To form the crRNA:tracrRNA duplexes (i.e., the guide RNAs [gRNAs]), IDT nuclease-free duplex buffer (IDT, Coralville, IA, USA) was used according to the instructions of the manufacturer. Deletion cassettes functioning also as the template DNAs for the HDR were constructed by PCR using the Phusion Flash high-fidelity PCR master mix (Thermo Fisher Scientific, Waltham, MA, USA). First, two fragments upstream and downstream from the protospacer sequence of the corresponding *cotH* gene and the entire *pyrG* gene along with its promoter and terminator sequences were amplified using the primers listed in Table S1B. The amplified fragments were fused in a subsequent PCR using nested primers (Table S1B) where the ratio of concentrations of the fragments was 1:1:1. For each transformation procedure, 5 μg template DNA, 10 μM gRNA, and 10 μM Cas9 nuclease enzyme (Alt-R S.p. Cas9 nuclease; IDT, Coralville, IA, USA) were introduced together into the *M. lusitanicus* MS12 strain by polyethylene glycol (PEG)-mediated protoplast transformation (29, 62). Potential mutant colonies were selected on solid YNB medium by complementing the uracil auxotrophy of the MS12 strain. From each primary transformant, monosporangial colonies were formed under selective conditions. Disruption of the *cotH* genes and the presence of the integrated *pyrG* gene were proven by PCR using the primers listed in Table S1B and sequencing of the amplified fragment. Sequencing and PCR revealed that the CRISPR-Cas9-mediated HDR caused the expected modification (i.e., disruption of the *cotH* genes by the integration of the *pyrG*) in the targeted sites. Real-time quantitative reverse transcription-PCR (qRT-PCR) analysis indicated the lack of *cotH* transcripts in all transformants.

Complementation. To complement the knockout of the *cotH3* and the *cotH4* genes, autonomously replicating vectors were used, where the complementing gene constructs were maintained episomally. *cotH3* and *cotH4* with their promoter and terminator sequences were amplified by PCR using the Phusion Flash high-fidelity PCR master mix (Thermo Scientific) and the primer pairs *McCotH3_compl_fw* and *McCotH3_compl_rev* and *McCotH4_compl_fw* and *McCotH4_compl_rev*, respectively, and were ligated separately into pJet1.2 cloning vectors (Thermo Scientific), resulting in the constructs pJet1.2-McCotH3 and pJet1.2-McCotH4, respectively. We further ensured that a unique rare-cutting restriction site is present in both plasmids (NotI), which should facilitate easy insertion of complementing genes. We have therefore combined in a single vector the auxotrophic selection marker *leuA*, allowing primary selection of numerous transformants with our gene of interest, resulting in plasmids pMCcotH3leuAcomp and pMCcotH4leuAcomp. The plasmid construct was introduced to the MS12-Δ*cotH3*+*pyrG* and MS12-Δ*cotH4*+*pyrG* disruption strains by PEG-protoplast transformation. In experiments with a plasmid for complementation of *cotH3* and *cotH4* gene deletion, 3 μg DNA was added to the protoplasts in a transformation reaction mixture. Transformants were transferred to minimal media (YNB), considering the phenomenon of complementation of auxotrophy after successful transformation, and confirmed by PCR and qPCR. The selection method is based on the complementation of the leucine auxotrophy. The created knockout and complemented *M. lusitanicus* strains are listed in Table S2B.

Electron microscopy and quantitative analysis of the wall thickness. Pellets from isolated spores were immersed into a 2% paraformaldehyde (Sigma, St. Louis, MO, USA) and 2.5% glutaraldehyde (Polysciences, Warrington, PA, USA) containing modified Karnovsky fixative in phosphate buffer. The pH of the solution was adjusted to 7.4. Samples were fixed overnight at 4°C, then briefly rinsed in distilled water (pH 7.4) for 10 min and fixed in 2% osmium tetroxide (Sigma-Aldrich, St. Louis, MO, USA) in distilled water (pH 7.4) for 60 min. After osmification, samples were rinsed in distilled water for 10 min again then dehydrated using a graded series of ethanol (Molar, Halasztelek, Hungary) from 50% to 100% for 10 min in each. Afterwards, all spore pellets were proceeded through in propylene oxide (Molar, Halasztelek, Hungary) and then embedded in an epoxy-based resin, Durcupan ACM (Sigma-Aldrich, St. Louis, MO, USA). After polymerization for 48 h at 56°C, resin blocks were etched, and 50-nm-thick ultrathin sections were cut on an Ultracut UCT ultramicrotome (Leica, Wetzlar, Germany). Sections were mounted on a single-hole, Formvar-coated copper grid (Electron Microscopy Sciences, Hatfield, PA, USA). For a better signal-to-noise ratio, 2% uranyl acetate (Electron Microscopy Sciences) (in 50% ethanol from Molar, Halasztelek, Hungary) and 2% lead citrate (in distilled water from Electron Microscopy Sciences, Hatfield, PA, USA) were used. Ultrathin sections from the pellets were screened at a magnification of $\times$1,000 to $\times$3,000 on a JEM-1400 Flash transmission electron microscope (JEOL, Tokyo, Japan) until 70 individual spore cross sections were identified from each sample. For quantitative measurements of the major and minor axes, images with area and circularity of a $\times$1,000 to $\times$3,000 magnification were used. For the thickness measurements of the different layers of the spore wall (Fig. 5D), images were recorded at $\times$10,000 magnification using a 2k $\times$ 2k Matataki (JEOL, Tokyo, Japan) scientific complementary metal oxide-semiconductor camera. All the quantitative data were determined using the built-in measurements module of the TEM Center software (JEOL, Tokyo, Japan).

Fluorescence staining. Four-day-old fungal spores were collected from MEA and washed three times with 1$\times$ sterile phosphate buffered saline (PBS) (137 mM NaCl, 2.7 mM KCl, 10 mM Na_2HPO_4, 2 mM KH_2PO_4 [pH 7.4]) and were collected by centrifugation for 10 min at 4°C at 2,000 $\times$ *g* followed by another centrifugation step using the same conditions for 5 min. The pellet was resuspended in 0.5 mL of 1% (wt/vol) bovine serum albumin (BSA) (Gibco) solution and incubated for 30 min at room temperature with constant rotation. Fungal spores (10^7/mL) were washed three times with 1$\times$ PBS and then stained for 45 min in PBS containing 5 μg/mL CFW solution or 100 μg/mL ConA-FITC solution. After staining, samples were washed five times with PBS. For analysis, collected samples were centrifuged at 2,000 $\times$ *g* for 15 min and resuspended in 200 μL PBS supplemented with 0.05% Tween 20 (Reanal, Budapest, Hungary). Fluorescence images of the stained fungal cells were taken with a Zeiss Axioscope 40 microscope and an Axiocam Mrc camera. Filters at 350-nm excitation and 432-nm emission were used to detect chitin, while

filters at 495-nm excitation and 515-nm emission were used after ConA-FITC staining. Samples were also measured with a FlowSight imaging flow cytometer (Amnis ImageStream X Mk II imaging flow cytometer; Amnis, Austin, TX, USA), and the associated IDEAS 6.2 software (63) was used for evaluation. For samples prepared by fluorescence microscopy, the intensity of the dyes for the different strains was determined using ImageJ2 (Fiji) (64). The mean fluorescence intensity of CFW was determined by microscopy. Significance was determined by unpaired *t* test.

Interactions of *M. lusitanicus* with macrophages. The murine macrophage cell line J774.2 was cultivated in Dulbecco's minimal essential medium (DMEM) (Lonza, Basel, Switzerland) supplemented with 10% heat-inactivated fetal bovine serum (FBS) (Biosera, Kansas City, MO, USA) and 1% penicillin–streptomycin solution (Sigma-Aldrich, St. Louis, MO, USA) at 37°C, 5% CO_2, and 100% relative humidity. The same medium was used in all the interaction experiments. Four hours before the experiment, J774.2 cells (2×10^5 cells/mL) were freshly harvested and stained with CellMask deep red plasma membrane stain (Thermo Fisher Scientific, Waltham, MA, USA) following the instructions of the manufacturer, and then seated on a 24-well plate. Fungal spores were freshly collected from 1-week-old MEA cultures and stained with Alexa Fluor 488, carboxylic acid, and succinimidyl ester (Invitrogen, Waltham, MA, USA). Labeled macrophages and spores were coincubated at a multiplicity of infection (MOI) of 5:1 for 90 min at 37°C and 5% CO_2. For analysis, collected samples were centrifuged with $1,000 \times g$ for 10 min and then resuspended in 200 μL PBS supplemented with 0.05% Tween 20. Interaction and phagocytosis were measured using a FlowSight imaging flow cytometer (Amnis ImageStream X Mk II imaging flow cytometer; Amnis, Austin, TX, USA) and evaluated with IDEAS software (Amnis ImageStream X Mk II imaging flow cytometer; Amnis, Austin, TX, USA). Data from 10,000 events per sample were collected and analyzed. The number of engulfed cells was determined by examining 200 images of individual macrophages, while the phagocytic index (PI) was determined using the following formula: PI = (mean spore count per phagocytosing cell) $\times$ (% of phagocytosing cells containing at least one fungal spore).

To analyze the phagosome acidification of J774.2 cells by flow cytometry, fungal spores were labeled with pHrodo Red succinimidyl ester (Invitrogen, Waltham, MA, USA), according to the manufacturer's instructions. CellMask Deep Red Plasma Membrane stain (Thermo Ficher Scientific, Waltham, MA, USA) labeled macrophages and FITC labeled spores were coincubated at an MOI of 5:1, for 120 min at 37°C and 5% CO_2. The ratio of the phagocytosing cells was also determined at 120 min under the same conditions of interactions, except the fungal spores were stained with CFW. Phagosome acidification was calculated as follows: [(% of pHrodo Red^+ cells)/(% of phagocytosing cells)] $\times$ 100.

To assay the survival of the fungal spores, the interaction of J774.2 cells and the spores was performed at an MOI of 5:1 for 180 min. After the interaction, cells and spores were collected and macrophages were lysed with sterile distilled water. Serial dilutions were prepared from the spore suspensions and plated on MEA to quantify the CFU. Survival of spores was calculated using the following formula: survival = ($CFU_{interaction} \times 100$)/$CFU_{control}$, where $CFU_{interaction}$ is the CFU of samples coincubated with macrophages, while $CFU_{control}$ is the CFU of control samples, incubated under the same conditions but without macrophages.

Survival assay in *Drosophila melanogaster*. *Drosophila* stocks were raised and kept following the infection on standard cornmeal agar medium at 28°C. Spore suspensions were prepared in sterile PBS from 7-day-old cultures grown on YNB plates (supplemented with 0.5 g/L leucine, if required) at 28°C. The *Drosophila* Oregon R strain, originally obtained from the Bloomington Drosophila Stock Center (Bloomington, IN, USA), was used throughout the experiments. Infection was performed by dipping a thin needle in a suspension of fungal conidia (10^7 conidia/mL) or PBS as the uninfected control, and subsequently, the thorax of the anaesthetized fly was collected. Flies were counted at different times to monitor survival. Flies were moved into fresh vials every other day. Each experiment was performed with 60 flies. The results shown are representative of at least three independent experiments.

Survival assay in *Galleria mellonella* larvae. Spores were resuspended in insect physiological saline (IPS) (50 mM NaCl, 5 mM KCl, 10 mM EDTA and 30 mM sodium citrate in 0.1 M Tris-HCl [pH 6.9]) (65). *G. mellonella* larvae (TruLarv; BioSystems Technology) were inoculated with 10^5 fungal cells in 20 μL IPS via the last proleg using 29-gauge insulin needles (BD Micro-Fine). For each *M. lusitanicus* strain, 20 larvae were infected. For IPS-treated (uninfected) and witness controls (no injections, uninfected), 20 animals were utilized too. Larvae were maintained at 28°C, and their survival was monitored daily for 6 days. The results shown are representative of at least three independent experiments.

***In vivo* virulence studies in diabetic ketoacidotic (DKA) mouse model.** Male ICR (CD-1) outbred mice ($\geq$20 g) were all purchased from Envigo and housed in groups of 8 each. Mice were rendered DKA with a single intraperitoneal injection of 190 mg/kg streptozocin in 0.2 mL citrate buffer (pH 4.2) 10 days before the fungal challenge. Glycosuria and ketonuria were confirmed in all mice 7 days after streptozocin treatment. Furthermore, on days -2 and $+3$ relative to infection, mice were given a dose of cortisone acetate (250 mg/kg subcutaneously [s.c.]). Mice were given 50 ppm enrofloxacin (Baytril; Bayer) added to the drinking water from day -3 to day 0 *ad libitum*. Ceftazidine antibiotics were added (5 mg/dose/0.2 mL s.c.) from day 0 and continued until day $+8$. DKA mice were infected intratracheally with a target inoculum of 2.5×10^6 fresh spores (1×10^8 spores/mL) in 25 μL PBS after sedation with isoflurane gas.

Ethics statement. All animal studies were approved by the Institutional Animal Care and Use Committee (IACUC) of the Los Angeles Biomedical Research Institute at Harbor-UCLA Medical Center according to the NIH guidelines for animal housing and care (project 11671).

Statistical analysis. All measurements were performed in at least two technical and three biological replicates. Statistical significance was analyzed by *t* tests or one-way analysis of variance (ANOVA) followed by Dunnett's multiple-comparison test using Microsoft Excel of the Microsoft Office package or GraphPad Prism 7.00 (GraphPad Software, La Jolla, California USA) as appropriate. *P* values of <0.05 were considered

statistically significant. In *in vivo* survival experiments, differences between the pathogenicity of the fungal strains were compared by the log rank test. *P* values of <0.05 were considered statistically significant.

SUPPLEMENTAL MATERIAL

Supplemental material is available online only.

FIG S1, TIF file, 2.6 MB.
FIG S2, TIF file, 2.1 MB.
FIG S3, TIF file, 2.5 MB.
FIG S4, TIF file, 2 MB.
FIG S5, TIF file, 0.2 MB.
FIG S6, TIF file, 2.6 MB.
FIG S7, TIF file, 1.9 MB.
TABLE S1, XLSX file, 0.01 MB.
TABLE S2, XLSX file, 0.01 MB.
DATA SET S1, XLSX file, 0.04 MB.

ACKNOWLEDGMENTS

This study was supported by grants NKFIA K131796, ELKH 2001007, and ITM NKFIA TKP-2021-EGA-28 to T.P. and by the Public Health Service grant R01 AI063503 to A.S.I. Publication was supported by the University of Szeged Open Access Fund (grant no. 5752). G.N. is grateful for the support of the Premium Postdoctoral Fellowship Program of the Hungarian Academy of Sciences (460050). C.S. is supported by the ÚNKP-20-4-I and ÚNKP-22-4-SZTE-523 New National Excellence Program of the Ministry for Innovation and Technology from the source of the National Research, Development and Innovation Fund. R.P. and K.S. were supported by the "National Talent Program" with the financial aid of the Ministry of Human Capacities (NTP-NFTÖ-22-B-0027 and NTP-NFTÖ-22-B-0069).

We thank Szilárd Szebenyi for help with creating the figures. We are grateful to Victoriano Garre and DoE JGI for contributing the unpublished data of the *Mucor lusitanicus* CBS277.49 v.3.0 genome used in the phylogenetic analysis of the *cotH* sequences. Sequence data were produced by the U.S. Department of Energy Joint Genome Institute (https://www.jgi.doe.gov/) in collaboration with the user community. The work conducted by the U.S. Department of Energy Joint Genome Institute, a DOE Office of Science User Facility, is supported by the Office of Science of the U.S. Department of Energy under contract no. DE-AC02-05CH11231.

A.S.I. owns shares in Vitalex Biosciences, a start-up company that is developing immunotherapies and diagnostics for mucormycosis. The remaining authors declare no conflict of interest.

Resources were provided by T.P., G.N., R.P., R.S., U.B., and A.S.I. Conceptualization, methodology and supervision were performed by T.P., G.N., A.S.I., and C.V. Validation of the results, writing, supervising, and editing the manuscript were carried out by T.P., C.S., G.N., R.P., R.S., A.S.I., and C.V. Investigation was performed by C.S., S.K.-V., O.J., Y.G., T.G., K.S., M.H., U.B. Figures and tables were arranged by C.S., S.K., R.P., and A.S.I. All authors collected data, provided resources, participated in data curation and formal analysis, and/or contributed to the revision of the manuscript.

REFERENCES

1. Gebremariam T, Alkhazraji S, Soliman SSM, Gu Y, Jeon HH, Zhang L, French SW, Stevens DA, Edwards JE, Filler SG, Uppuluri P, Ibrahim AS. 2019. Anti-CotH3 antibodies protect mice from mucormycosis by prevention of invasion and augmenting opsonophagocytosis. Sci Adv 5:eaaw1327. https://doi.org/10.1126/sciadv.aaw1327.
2. Walther G, Wagner L, Kurzai O. 2020. Outbreaks of Mucorales and the species involved. Mycopathologia 185:765–781. https://doi.org/10.1007/s11046-019-00403-1.
3. Prakash H, Chakrabarti A. 2019. Global epidemiology of mucormycosis. J Fungi (Basel) 5:26. https://doi.org/10.3390/jof5010026.
4. Skiada A, Lass-Floerl C, Klimko N, Ibrahim A, Roilides E, Petrikkos G. 2018. Challenges in the diagnosis and treatment of mucormycosis. Med Mycol 56:93–101. https://doi.org/10.1093/mmy/myx101.
5. Jeong W, Keighley C, Wolfe R, Lee WL, Slavin MA, Kong DCM, Chen SC-A. 2019. The epidemiology and clinical manifestations of mucormycosis: a systematic review and meta-analysis of case reports. Clin Microbiol Infect 25:26–34. https://doi.org/10.1016/j.cmi.2018.07.011.
6. Riley TT, Muzny CA, Swiatlo E, Legendre DP. 2016. Breaking the mold: a review of mucormycosis and current pharmacological treatment options. Ann Pharmacother 50:747–757. https://doi.org/10.1177/1060028016655425.

7. Lanternier F, Dannaoui E, Morizot G, Elie C, Garcia-Hermoso D, Huerre M, Bitar D, Dromer F, Lortholary O. French Mycosis Study Group. 2012. A global analysis of mucormycosis in France: the RetroZygo study (2005–2007). Clin Infect Dis 54(Suppl 1):S35–S43. https://doi.org/10.1093/cid/cir880.
8. Garcia A, Vellanki S, Lee SC. 2018. Genetic tools for investigating Mucorales fungal pathogenesis. Curr Clin Microbiol Rep 5(Suppl 1):173–180. https://doi.org/10.1007/s40588-018-0097-7.
9. Gomes MZR, Lewis RE, Kontoyiannis DP. 2011. Mucormycosis caused by unusual Mucormycetes, non-*Rhizopus*, -*Mucor*, and -*Lichtheimia* species. Clin Microbiol Rev 24:411–445. https://doi.org/10.1128/CMR.00056-10.
10. Skiada A, Lanternier F, Groll AH, Pagano L, Zimmerli S, Herbrecht R, Lortholary O, Petrikkos GL. European Conference on Infections in Leukemia. 2013. Diagnosis and treatment of mucormycosis in patients with hematological malignancies: guidelines from the 3rd European Conference on Infections in Leukemia (ECIL 3). Haematologica 98:492–504. https://doi.org/10.3324/haematol.2012.065110.
11. Reid G, Lynch JP, Fishbein MC, Clark NM. 2020. Mucormycosis. Semin Respir Crit Care Med 41:99–114. https://doi.org/10.1055/s-0039-3401992.
12. do Monte Junior ES, dos Santos MEL, Ribeiro IB, Luz GdO, Baba ER, Hirsch BS, Funari MP, de Moura EGH. 2020. Rare and fatal gastrointestinal mucormycosis (zygomycosis) in a COVID-19 patient: a case report. Clin Endosc 53:746–749. https://doi.org/10.5946/ce.2020.180.
13. Mehta S, Pandey A. 2020. Rhino-orbital mucormycosis associated with COVID-19. Cureus 12:e10726. https://doi.org/10.7759/cureus.10726.
14. Werthman-Ehrenreich A. 2021. Mucormycosis with orbital compartment syndrome in a patient with COVID-19. Am J Emerg Med 42:264.e5–264.e8. https://doi.org/10.1016/j.ajem.2020.09.032.
15. Naclerio G, Baccigalupi L, Zilhao R, De Felice M, Ricca E. 1996. *Bacillus subtilis* spore coat assembly requires *cotH* gene expression. J Bacteriol 178:4375–4380. https://doi.org/10.1128/jb.178.15.4375-4380.1996.
16. Nguyen KB, Sreelatha A, Durrant ES, Lopez-Garrido J, Muszewska A, Dudkiewicz M, Grynberg M, Yee S, Pogliano K, Tomchick DR, Pawłowski K, Dixon JE, Tagliabracci VS. 2016. Phosphorylation of spore coat proteins by a family of atypical protein kinases. Proc Natl Acad Sci U S A 113:E3482–E3491. https://doi.org/10.1073/pnas.1605917113.
17. Scott JD, Newton AC. 2016. Bacterial spore coat protein kinases: a new twist to an old story. Proc Natl Acad Sci U S A 113:6811–6812. https://doi.org/10.1073/pnas.1607004113.
18. Freitas C, Plannic J, Isticato R, Pelosi A, Zilhão R, Serrano M, Baccigalupi L, Ricca E, Elsholz AKW, Losick R, Henriques AO. 2020. A protein phosphorylation module patterns the *Bacillus subtilis* spore outer coat. Mol Microbiol 114:934–951. https://doi.org/10.1111/mmi.14562.
19. Gebremariam T, Liu M, Luo G, Bruno V, Phan QT, Waring AJ, Edwards JE, Filler SG, Yeaman MR, Ibrahim AS. 2014. CotH3 mediates fungal invasion of host cells during mucormycosis. J Clin Invest 124:237–250. https://doi.org/10.1172/JCI71349.
20. Chibucos MC, Soliman S, Gebremariam T, Lee H, Daugherty S, Orvis J, Shetty AC, Crabtree J, Hazen TH, Etienne KA, Kumari P, O'Connor TD, Rasko DA, Filler SG, Fraser CM, Lockhart SR, Skory CD, Ibrahim AS, Bruno VM. 2016. An integrated genomic and transcriptomic survey of mucormycosis-causing fungi. Nat Commun 7:12218. https://doi.org/10.1038/ncomms12218.
21. Ma L-J, Ibrahim AS, Skory C, Grabherr MG, Burger G, Butler M, Elias M, Idnurm A, Lang BF, Sone T, Abe A, Calvo SE, Corrochano LM, Engels R, Fu J, Hansberg W, Kim J-M, Kodira CD, Koehrsen MJ, Liu B, Miranda-Saavedra D, O'Leary S, Ortiz-Castellanos L, Poulter R, Rodriguez-Romero J, Ruiz-Herrera J, Shen Y-Q, Zeng Q, Galagan J, Birren BW, Cuomo CA, Wickes BL. 2009. Genomic analysis of the basal lineage fungus *Rhizopus oryzae* reveals a whole-genome duplication. PLoS Genet 5:e1000549. https://doi.org/10.1371/journal.pgen.1000549.
22. Alqarihi A, Gebremariam T, Gu Y, Swidergall M, Alkhazraji S, Soliman SSM, Bruno VM, Edwards JE, Filler SG, Uppuluri P, Ibrahim AS. 2020. GRP78 and integrins play different roles in host cell invasion during mucormycosis. mBio 11:e01087-20. https://doi.org/10.1128/mBio.01087-20.
23. Liu M, Spellberg B, Phan QT, Fu Y, Fu Y, Lee AS, Edwards JE, Filler SG, Ibrahim AS. 2010. The endothelial cell receptor GRP78 is required for mucormycosis pathogenesis in diabetic mice. J Clin Invest 120:1914–1924. https://doi.org/10.1172/JCI42164.
24. Baldin C, Soliman SSM, Jeon HH, Alkhazraji S, Gebremariam T, Gu Y, Bruno VM, Cornely OA, Leather HL, Sugrue MW, Wingard JR, Stevens DA, Edwards JE, Ibrahim AS. 2018. PCR-based approach targeting Mucorales-specific gene family for diagnosis of mucormycosis. J Clin Microbiol 56:e00746-18. https://doi.org/10.1128/JCM.00746-18.
25. Wagner L, Stielow JB, de Hoog GS, Bensch K, Schwartze VU, Voigt K, Alastruey-Izquierdo A, Kurzai O, Walther G. 2020. A new species concept for the clinically relevant *Mucor circinelloides* complex. Persoonia 44:67–97. https://doi.org/10.3767/persoonia.2020.44.03.
26. Li CH, Cervantes M, Springer DJ, Boekhout T, Ruiz-Vazquez RM, Torres-Martinez SR, Heitman J, Lee SC. 2011. Sporangiospore size dimorphism is linked to virulence of *Mucor circinelloides*. PLoS Pathog 7:e1002086. https://doi.org/10.1371/journal.ppat.1002086.
27. Lee SC, Li A, Calo S, Heitman J. 2013. Calcineurin plays key roles in the dimorphic transition and virulence of the human pathogenic zygomycete *Mucor circinelloides*. PLoS Pathog 9:e1003625. https://doi.org/10.1371/journal.ppat.1003625.
28. Lee SC, Li A, Calo S, Inoue M, Tonthat NK, Bain JM, Louw J, Shinohara ML, Erwig LP, Schumacher MA, Ko DC, Heitman J. 2015. Calcineurin orchestrates dimorphic transitions, antifungal drug responses and host-pathogen interactions of the pathogenic mucoralean fungus *Mucor circinelloides*. Mol Microbiol 97:844–865. https://doi.org/10.1111/mmi.13071.
29. Nagy G, Szebenyi C, Csernetics Á, Vaz AG, Tóth EJ, Vágvölgyi C, Papp T. 2017. Development of a plasmid free CRISPR-Cas9 system for the genetic modification of *Mucor circinelloides*. Sci Rep 7:16800. https://doi.org/10.1038/s41598-017-17118-2.
30. Chang Z, Heitman J. 2019. Drug-resistant epimutants exhibit organ-specific stability and induction during murine infections caused by the human fungal pathogen *Mucor circinelloides*. mBio 10:e02579-19. https://doi.org/10.1128/mBio.02579-19.
31. Vellanki S, Garcia AE, Lee SC. 2020. Interactions of FK506 and rapamycin with FK506 binding protein 12 in opportunistic human fungal pathogens. Front Mol Biosci 7:588913. https://doi.org/10.3389/fmolb.2020.588913.
32. Zilhão R, Naclerio G, Henriques AO, Baccigalupi L, Moran CP, Ricca E. 1999. Assembly requirements and role of CotH during spore coat formation in *Bacillus subtilis*. J Bacteriol 181:2631–2633. https://doi.org/10.1128/JB.181.8.2631-2633.1999.
33. Prakash H, Skiada A, Paul RA, Chakrabarti A, Rudramurthy SM. 2021. Connecting the dots: interplay of pathogenic mechanisms between COVID-19 disease and mucormycosis. J Fungi (Basel) 7:616. https://doi.org/10.3390/jof7080616.
34. Sabirli R, Koseler A, Goren T, Turkcuer I, Kurt O. 2021. High GRP78 levels in Covid-19 infection: a case-control study. Life Sci 265:118781. https://doi.org/10.1016/j.lfs.2020.118781.
35. Lebreton A, Meslet-Cladière L, Morin-Sardin S, Coton E, Jany J-L, Barbier G, Corre E. 2019. Comparative analysis of five *Mucor* species transcriptomes. Genomics 111:1306–1314. https://doi.org/10.1016/j.ygeno.2018.09.003.
36. Watkins TN, Gebremariam T, Swidergall M, Shetty AC, Graf KT, Alqarihi A, Alkhazraji S, Alsaadi AI, Edwards VL, Filler SG, Ibrahim AS, Bruno VM. 2018. Inhibition of EGFR signaling protects from mucormycosis. mBio 9:e01384-18. https://doi.org/10.1128/mBio.01384-18.
37. Ram AFJ, Klis FM. 2006. Identification of fungal cell wall mutants using susceptibility assays based on calcofluor white and Congo Red. Nat Protoc 1:2253–2256. https://doi.org/10.1038/nprot.2006.397.
38. Rodrigues J, Fonseca FL, Schneider RO, Godinho RM, Firacative C, Maszewska K, Meyer W, Schrank A, Staats C, Kmetzsch L, Vainstein MH, Rodrigues ML. 2015. Pathogenic diversity amongst serotype C VGIII and VGIV *Cryptococcus gattii* isolates. Sci Rep 5:11717. https://doi.org/10.1038/srep11717.
39. Garcia-Rubio R, de Oliveira HC, Rivera J, Trevijano-Contador N. 2019. The fungal cell wall: *Candida*, *Cryptococcus*, and *Aspergillus* species. Front Microbiol 10:2993. https://doi.org/10.3389/fmicb.2019.02993.
40. Bahn YS, Xue C, Idnurm A, Rutherford JC, Heitman J, Cardenas ME. 2007. Sensing the environment: lessons from fungi. Nat Rev Microbiol 5:57–69. https://doi.org/10.1038/nrmicro1578.
41. Pérez-Arques C, Navarro-Mendoza MI, Murcia L, Lax C, Martínez-García P, Heitman J, Nicolás FE, Garre V. 2019. *Mucor circinelloides* thrives inside the phagosome through an Atf-mediated germination pathway. mBio 10:e02765-18. https://doi.org/10.1128/mBio.02765-18.
42. Jacobsen ID. 2019. Animal models to study mucormycosis. J Fungi (Basel) 5:27. https://doi.org/10.3390/jof5020027.
43. Gottar M, Gobert V, Matskevich AA, Reichhart J-M, Wang C, Butt TM, Belvin M, Hoffmann JA, Ferrandon D. 2006. Dual detection of fungal infections in *Drosophila* through recognition of microbial structures and sensing of virulence factors. Cell 127:1425–1437. https://doi.org/10.1016/j.cell.2006.10.046.
44. Maurer E, Hörtnagl C, Lackner M, Grässle D, Naschberger V, Moser P, Segal E, Semis M, Lass-Flörl C, Binder U. 2019. *Galleria mellonella* as a model system to study virulence potential of mucormycetes and evaluation of antifungal treatment. Med Mycol 57:351–362. https://doi.org/10.1093/mmy/myy042.

45. López-Fernández L, Sanchis M, Navarro-Rodríguez P, Nicolás FE, Silva-Franco F, Guarro J, Garre V, Navarro-Mendoza MI, Pérez-Arques C, Capilla J. 2018. Understanding *Mucor circinelloides* pathogenesis by comparative genomics and phenotypical studies. Virulence 9:707–720. https://doi.org/10.1080/21505594.2018.1435249.
46. Benito EP, Díaz-Mínguez JM, Iturriaga EA, Campuzano V, Eslava AP. 1992. Cloning and sequence analysis of the *Mucor circinelloides pyrG* gene encoding orotidine-5′-monophosphate decarboxylase: use of *pyrG* for homologous transformation. Gene 116:59–67. https://doi.org/10.1016/0378-1119(92)90629-4.
47. Ibragimova S, Szebenyi C, Sinka R, Alzyoud EI, Homa M, Vágvölgyi C, Nagy G, Papp T. 2020. CRISPR-Cas9-based mutagenesis of the mucormycosis-causing fungus *Lichtheimia corymbifera*. Int J Mol Sci 21:3727. https://doi.org/10.3390/ijms21103727.
48. Gasteiger E, Hoogland C, Gattiker A, Duvaud S, Wilkins MR, Appel RD, Bairoch A. 2005. Protein identification and analysis tools on the ExPASy server, p 571–607. *In* Walker JM (ed), The proteomics protocols handbook. Humana Press, Totowa, NJ.
49. Grigoriev IV, Nikitin R, Haridas S, Kuo A, Ohm R, Otillar R, Riley R, Salamov A, Zhao X, Korzeniewski F, Smirnova T, Nordberg H, Dubchak I, Shabalov I. 2014. MycoCosm portal: gearing up for 1000 fungal genomes. Nucleic Acids Res 42:D699–D704. https://doi.org/10.1093/nar/gkt1183.
50. Quevillon E, Silventoinen V, Pillai S, Harte N, Mulder N, Apweiler R, Lopez R. 2005. InterProScan: protein domains identifier. Nucleic Acids Res 33:W116–W120. https://doi.org/10.1093/nar/gki442.
51. Punta M, Coggill PC, Eberhardt RY, Mistry J, Tate J, Boursnell C, Pang N, Forslund K, Ceric G, Clements J, Heger A, Holm L, Sonnhammer ELL, Eddy SR, Bateman A, Finn RD. 2012. The Pfam protein families database. Nucleic Acids Res 40:D290–D301. https://doi.org/10.1093/nar/gkr1065.
52. Steinegger M, Söding J. 2017. MMseqs2 enables sensitive protein sequence searching for the analysis of massive data sets. Nat Biotechnol 35:1026–1028. https://doi.org/10.1038/nbt.3988.
53. Katoh K, Standley DM. 2013. MAFFT multiple sequence alignment software version 7: improvements in performance and usability. Mol Biol Evol 30:772–780. https://doi.org/10.1093/molbev/mst010.
54. Nguyen L-T, Schmidt HA, von Haeseler A, Minh BQ. 2015. IQ-TREE: a fast and effective stochastic algorithm for estimating maximum-likelihood phylogenies. Mol Biol Evol 32:268–274. https://doi.org/10.1093/molbev/msu300.
55. Kalyaanamoorthy S, Minh BQ, Wong TK, von Haeseler A, Jermiin LS. 2017. ModelFinder: fast model selection for accurate phylogenetic estimates. Nat Methods 14:587–589. https://doi.org/10.1038/nmeth.4285.
56. Hoang DT, Chernomor O, von Haeseler A, Minh BQ, Vinh LS. 2018. UFBoot2: improving the ultrafast bootstrap approximation. Mol Biol Evol 35:518–522. https://doi.org/10.1093/molbev/msx281.
57. Sambrook J, Fritsch EF, Maniatis T. 1989. Molecular cloning: a laboratory manual, 2nd ed. Cold Spring Harbor Laboratory, Cold Spring Harbor, NY.
58. Alzohairy A. 2011. BioEdit: an important software for molecular biology. GERF Bull of Biosciences 2:60–61.
59. Corrochano LM, Kuo A, Marcet-Houben M, Polaino S, Salamov A, Villalobos-Escobedo JM, Grimwood J, Álvarez MI, Avalos J, Bauer D, Benito EP, Benoit I, Burger G, Camino LP, Cánovas D, Cerdá-Olmedo E, Cheng J-F, Domínguez A, Eliáš M, Eslava AP, Glaser F, Gutiérrez G, Heitman J, Henrissat B, Iturriaga EA, Lang BF, Lavín JL, Lee SC, Li W, Lindquist E, López-García S, Luque EM, Marcos AT, Martin J, McCluskey K, Medina HR, Miralles-Durán A, Miyazaki A, Muñoz-Torres E, Oguiza JA, Ohm RA, Olmedo M, Orejas M, Ortiz-Castellanos L, Pisabarro AG, Rodríguez-Romero J, Ruiz-Herrera J, Ruiz-Vázquez R, Sanz C, Schackwitz W, et al. 2016. Expansion of signal transduction pathways in fungi by extensive genome duplication. Curr Biol 26:1577–1584. https://doi.org/10.1016/j.cub.2016.04.038.
60. Livak KJ, Schmittgen TD. 2001. Analysis of relative gene expression data using real-time quantitative PCR and the $2^{-\Delta\Delta}CT$ method. Methods 25:402–408. https://doi.org/10.1006/meth.2001.1262.
61. Nagy G, Vaz AG, Szebenyi C, Takó M, Tóth EJ, Csernetics Á, Bencsik O, Szekeres A, Homa M, Ayaydin F, Galgóczy L, Vágvölgyi C, Papp T. 2019. CRISPR-Cas9-mediated disruption of the HMG-CoA reductase genes of *Mucor circinelloides* and subcellular localization of the encoded enzymes. Fungal Genet Biol 129:30–39. https://doi.org/10.1016/j.fgb.2019.04.008.
62. van Heeswijck R, Roncero MIG. 1984. High frequency transformation of *Mucor* with recombinant plasmid DNA. Carlsberg Res Commun 49:691–702. https://doi.org/10.1007/BF02907500.
63. Dominical V, Samsel L, McCoy JP. 2017. Masks in imaging flow cytometry. Methods 112:9–17. https://doi.org/10.1016/j.ymeth.2016.07.013.
64. Schindelin J, Arganda-Carreras I, Frise E, Kaynig V, Longair M, Pietzsch T, Preibisch S, Rueden C, Saalfeld S, Schmid B, Tinevez J-Y, White DJ, Hartenstein V, Eliceiri K, Tomancak P, Cardona A. 2012. Fiji: an open-source platform for biological-image analysis. Nat Methods 9:676–682. https://doi.org/10.1038/nmeth.2019.
65. Bergin D, Reeves EP, Renwick J, Wientjes FB, Kavanagh K. 2005. Superoxide production in *Galleria mellonella* hemocytes: identification of proteins homologous to the NADPH oxidase complex of human neutrophils. Infect Immun 73:4161–4170. https://doi.org/10.1128/IAI.73.7.4161-4170.2005.